

Potential science with GW250114 – the loudest binary black hole merger detected to date

Aleyna Akyüz[✉], Alex Correia[✉], Jada Garofalo[✉], Keisi Kacanja[✉], Labani Roy[✉], Kanchan Soni[✉], Hung Tan[✉], Vikas Jadhav Y[✉], and Alexander H. Nitz[✉]
Department of Physics, Syracuse University, Syracuse, NY 13244, USA

Collin D. Capano^{✉*}
*Department of Physics, Syracuse University, Syracuse, NY 13244, USA and
 Physics Department, University of Massachusetts Dartmouth, North Dartmouth, MA 02747, USA*
 (Dated: July 14, 2025)

On January 14, 2025 the LIGO interferometers detected a gravitational wave from the merger of two black holes, GW250114. Using publicly available information, we estimate that the signal-to-noise ratio (SNR) of GW250114 was ~ 80 . This would make it three to four times louder than any other gravitational wave detected to date. GW250114 therefore offers a unique opportunity to make precise measurements of its source parameters and to test general relativity. In anticipation of its public data release, we analyze a set of simulated signals that have parameters similar to what we estimate for GW250114 and explore what new insights may be gained from this significant event.

I. INTRODUCTION

The fourth observing run (O4) of Advanced LIGO [1], Virgo [2], and KAGRA [3] began on May 24, 2023. Since then,¹ the network of gravitational-wave (GW) detectors has collected over a year of data [4, 5]. The detector’s sensitivity during this period has been unprecedented: the luminosity distance at which a compact binary merger can be detected has more than doubled compared to the first observing run [4, 6]. This has led to a corresponding increase in the number of detections; a binary merger is now detected every ~ 3 days, yielding over 200 GW observations to date [5, 7].

Although the full O4 dataset has not yet been made public, the LIGO-Virgo-KAGRA (LVK) collaboration releases low-latency alerts for candidate events in near real-time [8]. These events facilitate rapid electromagnetic follow-ups and provide preliminary information about source classification and source properties such as sky location. In a companion paper [5], we show that it is also possible to estimate the signal-to-noise ratio (SNR) and the chirp mass of these events using the publicly available information.

On January 14, 2025, the LVK Collaboration identified a compact binary merger event GW250114, likely originating from the coalescence of a binary black hole (BBH)[7]. Based on our analysis of publicly available information [5], we estimate the SNR of GW250114 to be ~ 77 . This

makes it the loudest GW detected to date; it is ~ 3 times louder than GW150914 [9], which was the first and loudest BBH detected prior to O4. GW250114 thus provides an excellent opportunity to explore fundamental questions about BBH formation and allow for stringent tests of general relativity (GR).

In this work, we analyze a set of BBH simulations with properties similar to what we expect GW250114 to have, to highlight new insights that may be gained from this event. We investigate how well key physical properties of the system can be measured, such as its components’ masses and spins, as well as any potential eccentricity. We also perform tests of GR on these simulated signals to determine what constraints may be inferred from this event. These tests include a quasi-normal mode analysis of the post-merger signal (“Black hole spectroscopy”), a time-domain inspiral-merger-ringdown (IMR) consistency test, and a consistency test of sub-dominant modes evaluated over the entire observable signal (“BBH spectroscopy”). To perform these tests, we select a non-spinning numerical relativity (NR) simulation similar to GW150914 as our reference signal, with masses and distance rescaled to match the SNR of GW250114. We also generate simulations using the SEOBNRv5EHM [10] (to study eccentricity), and NRSur7dq4 [11] and IMRPhenomXPHM [12] (to study spin) waveform models.

All simulations are performed in a zero-noise realization of the Hanford and Livingston detectors, which were the observatories that detected the GW250114 [7]. We use the power spectral density (PSD) of each detector around the time of the event to evaluate the likelihood function while doing Bayesian inference. The PSDs are obtained by digitizing publicly available plots of the median PSD

* cdcapano@syr.edu

¹ As of May 2025.

measured over the day of the event [4]. All analyses are conducted with the latest version of PyCBC Inference [13, 14].

II. SOURCE CHARACTERIZATION

To establish a baseline for comparison, we use a simulation of a BBH merger from numerical relativity (NR) as our reference signal. Specifically, we use **SXS:BBH:3984** from the latest release of the Simulating eXtreme Spacetimes (SXS) catalog [15]. This simulation corresponds to a non-eccentric BBH merger with a mass ratio $q \equiv m_1/m_2 = 1.5$ and with nearly zero spins on each component. It also exhibits high numerical accuracy and convergence. To check its numerical accuracy, we compute the mismatch between the highest and second-highest resolution used in the NR simulations. We find that the mismatch is 1.24×10^{-5} , indicating excellent numerical convergence consistent with previously reported results [15, 16].

For our analysis, we rescale the total mass of the reference signal to $M = 69.923 M_\odot$, resulting in component masses of $m_1 = 41.954 M_\odot$ and $m_2 = 27.969 M_\odot$. We set the luminosity distance to $D_L = 440$ Mpc and the inclination angle $\iota = 36.6^\circ$, which corresponds to the most probable orientation. These masses, distance, and inclination are chosen to yield a network SNR of ~ 77 [5]. The sky location and luminosity distance are obtained from the maximum of the posterior distribution in the publicly available FITS files on the Gravitational-Wave Candidate Event Database (GraceDB) [7], as produced by Bilby [17].

To evaluate systematic uncertainties arising from waveform modeling, we perform Bayesian inference on this NR injection using the **IMRPhenomXPHM** [12] and **NRSur7dq4** [11] waveform models. A comparison of the recovery of chirp mass \mathcal{M} , mass ratio q , and effective spin χ_{eff} are shown in Fig. 1 and Table II. We find excellent agreement between the two models, and both models accurately recover the injected parameters, consistent with expectations for non-spinning signals [11, 12]. If GW250114 is non-spinning, systematic errors in waveform models should therefore be small relative to statistical errors.

A. Eccentricity

Orbital eccentricity describes the deviation of a binary's orbit from a perfect circle, and produces gravitational wave with distinctive phase and amplitude modulations [18]. Systems with

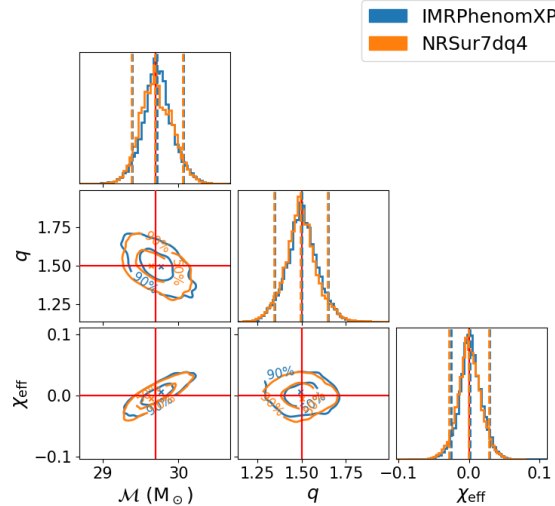


FIG. 1. Marginal posterior distributions on chirp mass \mathcal{M} , mass ratio q , and effective spin χ_{eff} of the reference NR simulation, obtained using **IMRPhenomXPHM** [12] (blue) and **NRSur7dq4** [11] (orange). The 50% and 90% credible regions are shown in the 2D marginal posterior plots; the middle 90% is indicated by the vertical dashed lines in the 1D marginal posteriors. Red lines indicate the injected values. Both models accurately recover the injected values.

non-negligible eccentricity can enter the detector band with residual eccentricity, which may be measurable and provide insights for the formation mechanisms of such binaries. In particular, high eccentricity is often associated with dynamical formation channels, such as interactions in dense stellar environments [19–22].

To investigate the measurability of eccentricity for an event like GW250114, we perform an injection study using the new eccentric aligned spin waveform model **SEOBNRv5EHM** [10]. We inject three dominant mode signals using the same intrinsic and extrinsic parameters as the reference injection, but with three different eccentricities $e = [0, 0.05, 0.1]$ at a reference frequency of 20 Hz, and a fixed radial anomaly of $l = \pi$, which is the angle that describes the position of the object in the eccentric orbit. Since the model does not account for precession, we fix the aligned spins to be 0. For Bayesian analysis, we use a uniform prior distribution for eccentricity, a uniform distribution for aligned spins, and a uniform angle on radial anomaly. Both the injections and subsequent Bayesian analyses are performed using **SEOBNRv5EHM**, allowing us to evaluate how well eccentricity can be constrained in each case.

We present our results in Fig. 2. We find that eccentricity is not measurably different from zero in the $e = 0$ injection, with the 90% credible

| Simulation | Model | \mathcal{M} [M_\odot] | q | M_{tot} [M_\odot] | χ_{eff} | χ_p |
|---------------------|--------------|-----------------------------|-------|--------------------------------|-------------------------|-----------------------|
| Reference | SXS:BBH:3984 | 29.699 | 1.500 | 69.923 | 0 | 0 |
| High Precession | NRSur7dq4 | 29.699 | 1.500 | 69.923 | -3.012×10^{-6} | 0.9 |
| Moderate Precession | NRSur7dq4 | 29.699 | 1.500 | 69.923 | 0.262 | 0.636 |
| Anti Aligned Spin | NRSur7dq4 | 29.699 | 1.500 | 69.923 | -0.680 | 2.87×10^{-9} |
| Non-Spinning | NRSur7dq4 | 29.699 | 1.500 | 69.923 | 0 | 0 |

TABLE I. Injected chirp mass \mathcal{M} , mass ratio q , total mass M_{tot} , effective spin χ_{eff} , and χ_p of the simulations. Values reported for chirp mass \mathcal{M} and total mass M_{tot} are in the detector frame.

TABLE II. Recovered parameters with 90% credible intervals for the simulations shown in Table II. Here, the Model column refers to the waveform model used to recover the simulation. Values reported for chirp mass \mathcal{M} and total mass M_{tot} are in the detector frame.

| Simulation | Model | \mathcal{M} [M_\odot] | q | M_{tot} [M_\odot] | χ_{eff} | χ_p |
|---------------------|---------------|-----------------------------|------------------------|--------------------------------|----------------------------|---------------------------|
| Reference | IMRPhenomXPHM | $29.72^{+0.35}_{-0.32}$ | $1.50^{+0.15}_{-0.15}$ | $69.98^{+0.84}_{-0.76}$ | $0.001^{+0.028}_{-0.027}$ | $0.070^{+0.146}_{-0.056}$ |
| Reference | NRSur7dq4 | $29.69^{+0.37}_{-0.31}$ | $1.49^{+0.16}_{-0.15}$ | $69.91^{+0.84}_{-0.81}$ | $0.000^{+0.028}_{-0.028}$ | $0.062^{+0.121}_{-0.049}$ |
| High Precession | NRSur7dq4 | $29.85^{+0.41}_{-0.32}$ | $1.48^{+0.16}_{-0.15}$ | $70.27^{+0.84}_{-0.82}$ | $0.009^{+0.039}_{-0.038}$ | $0.85^{+0.10}_{-0.11}$ |
| Moderate Precession | NRSur7dq4 | $29.67^{+0.35}_{-0.24}$ | $1.46^{+0.14}_{-0.15}$ | $69.67^{+1.16}_{-0.91}$ | $0.263^{+0.037}_{-0.025}$ | $0.59^{+0.25}_{-0.19}$ |
| Anti Aligned Spin | NRSur7dq4 | $29.87^{+0.59}_{-0.38}$ | $1.51^{+0.19}_{-0.17}$ | $70.4^{+1.2}_{-1.1}$ | $-0.660^{+0.054}_{-0.057}$ | $0.19^{+0.16}_{-0.11}$ |
| Non-Spinning | NRSur7dq4 | $29.73^{+0.29}_{-0.23}$ | $1.49^{+0.13}_{-0.14}$ | $69.97^{+0.76}_{-0.71}$ | $0.002^{+0.025}_{-0.024}$ | $0.060^{+0.120}_{-0.049}$ |

upper bound constrained to $e < 0.015$. For the $e = 0.05$ injection, the recovered posterior yields $e = 0.050^{+0.012}_{-0.012}$, tightly centered around the injected value and clearly excluding zero. This indicates that eccentricity at the level of 0.05 is distinguishable from a quasi-circular signal with current methods. The $e = 0.1$ injection is recovered as $e = 0.100^{+0.011}_{-0.011}$, also excluding zero and showing a strong deviation from circularity. These results suggest that eccentricities of $e \gtrsim 0.05$ may be detectable, while lower values, such as those consistent with zero, are not well measured.

B. Spin

The formation history of the BBH affects the orientation and magnitude of the spin of the initial black holes. For black holes formed via stellar collapse, the spin magnitude is influenced by the core-envelope coupling [23]. In contrast, black holes resulting from previous mergers are expected to have spin magnitudes around 0.7 [23]. The spin alignment depends on the formation environment of the binary, due to conservation of angular momentum. For instance, in dynamical environments, interactions with surrounding objects lead to an isotropic distribution of spin orientations, and spin precession is therefore expected. On the other hand, in isolated environments, the spins are expected to align with the orbital angular momentum, and precession is typically not observed [23].

To establish what spin constraints may be expected for GW250114 (and thus what can be

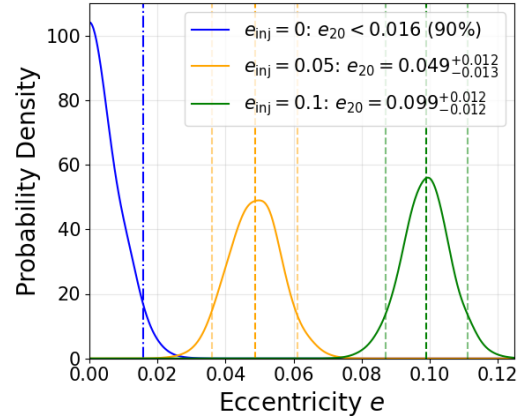


FIG. 2. Posterior distributions of orbital eccentricity for three injection studies of GW250114. The blue curve corresponds to the $e = 0$ injection, the orange to $e = 0.05$, and the green to $e = 0.1$ for a reference frequency of 20Hz. Each posterior is recovered using the SEOBNRv5EHM waveform model. Eccentricity cannot be bounded away from zero in the $e = 0$ case, while it is potentially measurable for the $e = 0.05$ and $e = 0.1$ injections.

gleaned about its formation history), we simulate four different scenarios: (1) non-spinning system; (2) a system with anti-aligned spin; (3) a system with high precession; (4) a system with moderate precession. The effective spin (χ_{eff}) and processing spin (χ_p) values for these scenarios are given in Table II.

The results can be seen in Fig. 3. For the

high-precession case, we can bound the primary spin amplitude to be higher than ~ 0.75 for NRSur7dq4 and ~ 0.5 for IMRPhenomXPHM analyses. For moderate precession, we can bound the primary spin amplitude to be higher than ~ 0.6 for NRSur7dq4 and ~ 0.7 for IMRPhenomXPHM. For the anti-aligned case, we only performed NRSur7dq4 analysis and obtained a lower bound of ~ 0.6 . For these analyses, secondary spin bounds are not significant. For the non-spinning case, the primary spin is bounded lower than ~ 0.15 and ~ 0.3 for the secondary. Even if GW250114 only has moderate precession, it should be possible to bound the magnitude of the secondary object's spin away from zero.

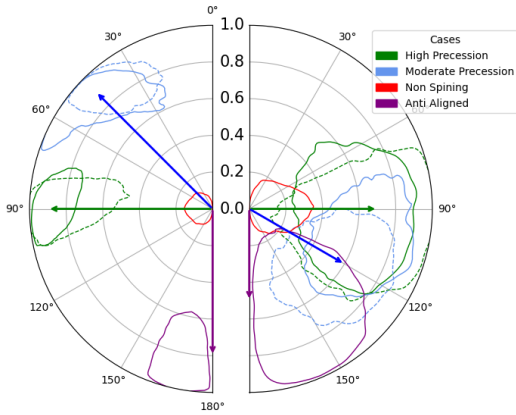


FIG. 3. 90% credible regions of the posterior distributions for the polar angle and spin magnitude of the primary (left) and secondary (right) objects. Arrows indicate the true injection values. Solid contours correspond to samples obtained using NR surrogate waveforms with injections from the same model, while dashed contours show results from IMRPhenomXPHM runs using identical injection parameters.

III. TESTS OF GENERAL RELATIVITY

A. Quasinormal mode detectability

Gravitational-wave observations allow for high-precision tests of GR in the strong-field regime of gravity. For example, we can perform “black hole spectroscopy” on the post-merger “ringdown” of binary black hole (BBH) coalescence. The ringdown of a BBH merger GW can be expressed as a superposition of quasinormal modes (QNM) specified by two angular indices $\ell \geq 2$, $m \leq |\ell|$, and an overtone number $n \geq 0$ [24, 25]. According to the no-hair theorem, the frequency and damping time measured for each mode should be maximally

determined by the mass and spin of the remnant BH. Inconsistencies between the measured QNMs and final mass and spin would imply inconsistencies with Kerr spacetime as predicted by GR [26].

We can test the no-hair theorem directly if a GW post-merger signal contains at least two detectable QNMs. With the exception of some highly precessing systems [27], the $(\ell, m, n) = (2, 2, 0)$ QNM is expected to be the dominant ringdown mode emitted by the black hole formed by a BBH merger. Several studies have claimed detection of subdominant modes in LVK data. Some authors claimed detection of a $(2, 2, 1)$ overtone in the ringdown of GW150914 and subsequently found agreement with the no-hair theorem [28–30]. Other analyses probed for the detectability of subdominant fundamental modes $(\ell, m \neq 2, n = 0)$ in the ringdown of GW190521 [31, 32].

Each analysis that claims subdominant mode detection — and even when the QNM model becomes a valid description of the post-merger — is hotly debated in the literature [33–41]. At least some of this contention is due to the choices of coalescence time (t_c) and sky location, which have traditionally been fixed due to technical challenges [29, 30, 42].

Correia *et al.* [42] developed methods to address these challenges and marginalize over the sky location and t_c uncertainty while performing a QNM analysis of the post-merger signal. The authors applied these methods to an analysis of GW150914 and found low evidence in favor of a $(2, 2, 0) + (2, 2, 1)$ model [43].

We employ the same methods of sky and time marginalization to probe the detectability of overtones in our model of GW250114. A full description of our methods is outlined in [42]. We test three QNM models: a baseline $(2, 2, 0)$ model, a $(2, 2, 0) + (2, 2, 1)$ model, and a $(2, 2, 0) + (2, 2, 1) + (2, 2, 2)$ model.

We calculate the Bayes factor $\mathcal{B}_{QNM} = Z_{QNM}/Z_{220}$ using the evidence Z for each model. For the one-overtone model, we obtain $\mathcal{B}_{221} = 2421$. Similarly, for the two-overtone model, we obtain $\mathcal{B}_{221+222} = 974$. These values indicate “decisive” [44] support for our injection to contain at least one detectable overtone. Figure 4 shows the amplitude and coalescence time posteriors for our analyses. Our one-overtone model posterior exhibits considerable support for A_{221} away from zero, thereby agreeing with the Bayes factor interpretation. Meanwhile, our two-overtone model exhibits more support for A_{222} away from zero and A_{221} at zero, and neither amplitude has as much support away from zero as the one-overtone model. These results suggest that only one overtone can be definitively detected in our injection.

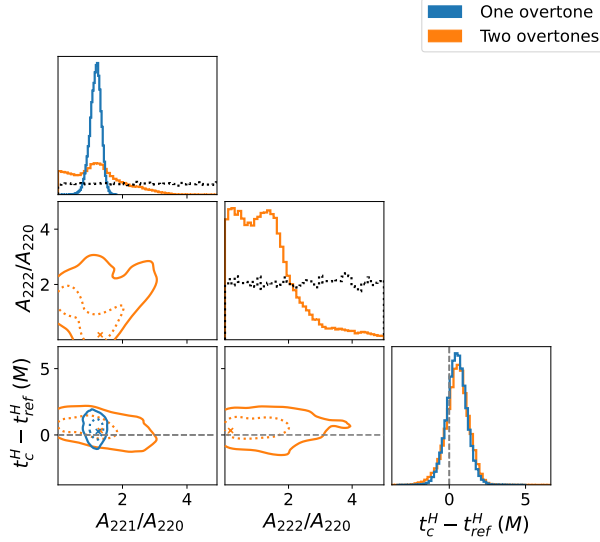


FIG. 4. The relative overtone amplitude and Hanford t_c posteriors for our QNM analyses. Results from the one-overtone $((2, 2, 0) + (2, 2, 1))$ ringdown and two-overtone $((2, 2, 0) + (2, 2, 1) + (2, 2, 2))$ ringdown models are indicated with blue and orange lines, respectively. Dotted and solid contours indicate the 50th and 90th percentiles of the posteriors, respectively. The maximum likelihood point in each 2D posterior is indicated with an X. Values of t_c are expressed relative to the injected Hanford t_c value in units of the final mass of our reference injection. A dashed gray line indicates the reference t_c of our injection. A dotted black line on each 1D histogram indicates the prior for the corresponding parameter.

We do not expect sub-dominant fundamental modes ($\ell, m \neq 2; n = 0$) to be detectable in GW250114. Fundamental modes are only expected to be observable in signals with high q or precession [27, 32, 45]. For our reference injection (with nonspinning progenitor BHs and $q \approx 1.5$), we estimate a total ringdown SNR of roughly 18, while the SNR of all other modes is around 2.1. Furthermore, none of the fundamental modes exceed an SNR of ~ 1.8 . This indicates a low probability of detecting fundamental modes in our reference signal. However, if the real data for GW250114 exhibits evidence for a high mass ratio ($q \gtrsim 4$) or precession effects, a fundamental QNM analysis will be warranted.

B. Time-domain IMR consistency

By independently measuring binary parameters from the pre- and post-merger signal, it is possible to test the consistency of observed events with the

laws of black hole thermodynamics [46]. Notably, we can test Hawking’s area theorem [47], which states that after coalescence of two black holes, the area of the final event horizon, A_f , must be greater than or equal to the sum of the horizon areas of the progenitor black holes, A_1 and A_2 :

$$A_1 + A_2 \equiv A_i \leq A_f. \quad (1)$$

It is a direct consequence of the second law of thermodynamics that the entropy of a black hole is proportional to its area [46]. If M is the mass and $\chi = J/M^2$ is the dimensionless spin of the black hole, then the area of a black hole is given by

$$A = 8\pi M^2(1 + \sqrt{1 - \chi^2}). \quad (2)$$

To test the area theorem, we use the ratio between the measured and expected changes in areas [48]

$$R = \frac{\Delta A_{\text{measured}}}{\Delta A_{\text{expected}}} = \frac{A_{f,\text{measured}} - A_i}{A_{f,\text{expected}} - A_i}. \quad (3)$$

$A_{f,\text{measured}}$ is measured from the final mass and spin estimated in the post-merger analysis. The component masses and spins prior to the merger are estimated from the inspiral (pre-merger) phase and then used to predict the final mass and spin via a NR fitting model. These predicted values are used to calculate the expected final horizon area $A_{f,\text{expected}}$ using Eq. (2). As $A_{f,\text{expected}}$ is derived from the NR model using the initial horizon areas A_1 and A_2 , the denominator of the test statistic R is positive definite. Therefore, if $R < 0$, it means that $A_{f,\text{measured}} < A_i$ and suggests a violation of the black hole area theorem. Furthermore, $R = 1$ indicates that the signal is consistent with GR.

$\Delta A_{\text{measured}}$ and $\Delta A_{\text{expected}}$ in Eq. (3) depend on the initial and final values of masses and spins, determined from the parameter estimation of pre and post merger part of the signal, respectively. Due to computational challenges in likelihood evaluation, earlier studies estimated these parameters while fixing sky location and t_c [48, 49]. However, this can lead to biases in the values of the measured parameters [50] and underestimate the statistical uncertainties [42]. A recent study [42] provided an approach to marginalize over sky-location and t_c , by simultaneously yet independently modeling the pre- and post-merger of the signal, allowing only sky-location and t_c to be shared between them. We consider the same approach of marginalization of the sky location and t_c to recover parameters and verify the area theorem.

The results of the area theorem test applied to the reference NR signal are shown in Fig. 5. We recover the parameters using the IMRPhenomXPHM waveform

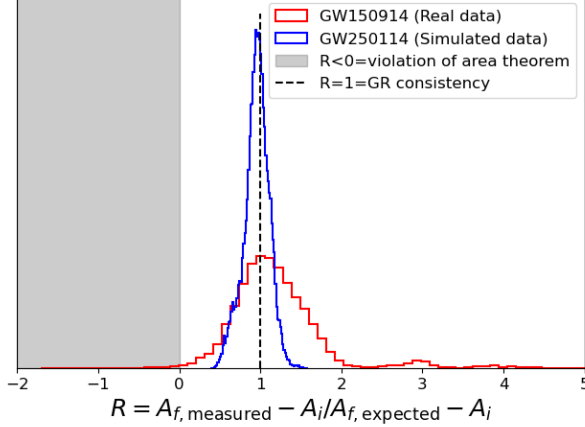


FIG. 5. Comparison area ratio plot R between GW150914 and GW250114. Blue distribution (GW250114) shows that a large fraction of posterior samples ($P(R > 0) = 100.00\%$) lie in the region $R > 0$, indicating strong consistency with the area theorem in comparison with red distribution (GW150914, $P(R > 0) = 99.36\%$) [42]

model. We find $R = 0.96^{+0.23}_{-0.30}$; as expected, this is a stronger constraint than GW150914, which yielded $R = 1.11^{+0.95}_{-0.63}$ using the same waveform model for the pre- and post-merger [42]. In particular, we find that the entirety of the posterior R is greater than zero. This observation indicates that it should be possible to confirm the area theorem (under the assumptions of this analysis) to very high confidence with GW250114. For comparison, $P(R > 0) = 99.36$ for GW150914 [42].

C. BBH spectroscopy

GW signals can be decomposed using spin-weighted spherical harmonics as follows,

$$h = h_+ - ih_\times = \frac{1}{D_L} \sum_{(l,m)} {}^{-2}Y_{lm}(\theta) e^{i(\psi_{lm}(\theta) + \Phi_c)}. \quad (4)$$

Each of these modes should be dependent only on the intrinsic parameters of the binary - the two masses, and spins. Thus, measurements of 2 or more harmonics would provide a way to measure any non-GR degrees of freedom. One way of doing this is using “BBH Spectroscopy” [51]. In this test, we add non-GR parameters for the higher modes, and treat them as free parameters to estimate. We look at deviations of the chirp mass, symmetric mass ratio and coalescence phase from the dominant (2,2) mode

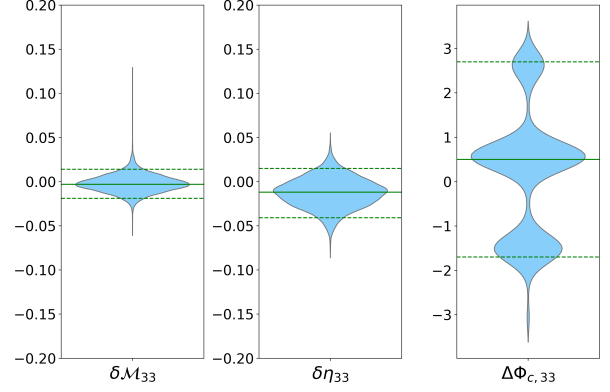


FIG. 6. Marginalized posteriors for the fractional deviations in chirp mass ($\delta\mathcal{M}_{33}$) symmetric mass ratio ($\delta\eta_{33}$), and the absolute deviation in the phase ($\Delta\Phi_{c,33}$) of the (3,3) mode from the (2,2) mode, with the median values (solid green) and credible intervals (dotted green). The results indicate consistency with GR within a 90% credible interval.

as our non-GR degrees of freedom.

$$\mathcal{M}_{lm} = \mathcal{M}_{22}(1 + \delta\mathcal{M}_{lm}), \quad (5)$$

$$\eta_{lm} = \eta_{22}(1 + \delta\eta_{lm}), \quad (6)$$

$$\Phi_{c,lm} = \Phi_{c,22} + \Delta\Phi_{c,lm}. \quad (7)$$

For our reference injection, the dominant modes in terms of SNR are the (2,2) mode with SNR = 86.92 followed by the (3,3) modes with SNR = 6.51. There also exists a small contribution from the (2,1) mode with an SNR = 2.36. We perform the BBH spectroscopy using only a higher (3,3) mode. We use IMRPhenomXPHM as the template waveform. We fix the spins to the reference injection values, as well as all extrinsic parameters except for inclination, since they affect each mode in the same way. We recover the masses, coalescence phase, and the deviations in them for the (3,3) mode.

The distributions for the fractional deviations in the (3,3) mode are shown in Fig. 6. We see that the deviations in mass parameters are $\delta\mathcal{M}_{33} = -0.005^{+0.017}_{-0.016}$ and $\delta\eta_{33} = -0.012^{+0.027}_{-0.029}$, are consistent with the predictions of GR. The measurement in the deviation in the coalescence phase does not provide a check of GR, but is consistent with (3,3) mode $\sim e^{i3\Phi_c}$, as the 90% credible interval, correspond to angles separated by $\sim 120^\circ$

IV. CONCLUSIONS

Dynamical formation of BBHs is hypothesized to occur in dense environments. BBHs formed

in this manner can potentially have non-zero eccentricity[52] when entering the GW detector band, non-aligned spins, and relatively high spin values[53, 54]. Our study shows that it may be possible to identify these effects in GW250114. Regarding eccentricity, we found that it should be possible to measure a non-zero eccentricity at 20 Hz in GW250114 if it has $e_{20} \gtrsim 0.05$. The dynamical formation channel also implies the isotropic spin orientation. We find that even in the case of moderate precession (i.e., with $\chi_p = 0.636$), it should be possible to exclude a non-spinning or aligned-spin scenario at the SNR of GW250114.

One of the most notable results of our study is that it should be possible to decisively measure an overtone of the dominant $(2, 2, 0)$ quasi-normal mode in the post-merger signal of GW250114, even when marginalizing over timing uncertainty. Previous detection claims of the overtone in GW150914 have been controversial due to the relatively large timing uncertainty [28, 30, 33, 43]. The SNR of GW250114 means that an overtone detection should be more clear cut, at least if it is non-spinning. However, even if an overtone is detectable, the question of whether or not a QNM model on its own is a valid description of the signal at merger will remain. Unfortunately, despite its overall large SNR, we do not believe any sub-dominant fundamental QNM modes will be detectable with this event.

Even if the GW250114 has a mass ratio as low as ~ 1.5 , it should be possible to measure and place constraints on deviations of the $(3, 3)$ mode from GR, as shown in Fig. 6. We also find that it should be possible to obtain excellent constraints on Hawking’s area theorem. We note, however, that the area-theorem constraint presented here is obtained with no gap in time between the pre-merger and post-merger measurement. A more rigorous test would be to measure the change in area between the early inspiral and post-merger. We will pursue this in a future study.

Our analysis suggests that GW250114 has the potential to offer many new insights into the formation of BBHs and into the fundamental physics that govern them. We look forward to the public data release of GW250114 so that we can confirm our predictions.

ACKNOWLEDGMENTS

AHN, KK, and KS acknowledge support from NSF grant PHY-2309240. CDC and AC acknowledge support from NSF grant PHY-2309356.

This research has used data or software obtained from the Gravitational Wave Open

Science Center (gwosc.org), a service of the LIGO Scientific Collaboration, the Virgo Collaboration, and KAGRA. This material is based upon work supported by NSF’s LIGO Laboratory which is a major facility fully funded by the National Science Foundation, as well as the Science and Technology Facilities Council (STFC) of the United Kingdom, the Max-Planck-Society (MPS), and the State of Niedersachsen/Germany for support of the construction of Advanced LIGO and construction and operation of the GEO600 detector. Additional support for Advanced LIGO was provided by the Australian Research Council. Virgo is funded, through the European Gravitational Observatory (EGO), by the French Centre National de Recherche Scientifique (CNRS), the Italian Istituto Nazionale di Fisica Nucleare (INFN) and the Dutch Nikhef, with contributions by institutions from Belgium, Germany, Greece, Hungary, Ireland, Japan, Monaco, Poland, Portugal, Spain. KAGRA is supported by Ministry of Education, Culture, Sports, Science and Technology (MEXT), Japan Society for the Promotion of Science (JSPS) in Japan; National Research Foundation (NRF) and Ministry of Science and ICT (MSIT) in Korea; Academia Sinica (AS) and National Science and Technology Council (NSTC) in Taiwan.

-
- [1] J. Aasi *et al.* (LIGO Scientific), “Advanced LIGO,” *Class. Quant. Grav.* **32**, 074001 (2015), arXiv:1411.4547 [gr-qc].
- [2] F. Acernese *et al.* (VIRGO), “Advanced Virgo: a second-generation interferometric gravitational wave detector,” *Class. Quant. Grav.* **32**, 024001 (2015), arXiv:1408.3978 [gr-qc].
- [3] T. Akutsu *et al.* (KAGRA), “KAGRA: 2.5 Generation Interferometric Gravitational Wave Detector,” *Nature Astron.* **3**, 35–40 (2019), arXiv:1811.08079 [gr-qc].
- [4] GWOSC developers, “Gravitational-wave observatory status,” https://gwosc.org/detector_status/.
- [5] Aleya Akyüz, Alex Correia, Keisi Kacanja, Vikas Jadhav Y, Labani Roy, Kanchan Soni, Hung Tan, Collin D. Capano, and Alexander H. Nitz, “Mining the alerts: A preliminary catalog of compact binaries from the fourth observing run,” In prep. (2025).
- [6] B. P. Abbott *et al.* (LIGO Scientific, Virgo), “GWTC-1: A Gravitational-Wave Transient Catalog of Compact Binary Mergers Observed by LIGO and Virgo during the First and Second Observing Runs,” *Phys. Rev. X* **9**, 031040 (2019), arXiv:1811.12907 [astro-ph.HE].
- [7] GraceDB Developers, “GraceDB,” <https://git.ligo.org/computing/gracedb>.
- [8] LIGO Scientific Collaboration, Virgo Collaboration, and KAGRA Collaboration, “Lvk em follow-up user guide,” <https://emfollow.docs.ligo.org/userguide/> (2023), accessed: 2025-06-23.
- [9] B. P. Abbott *et al.* (LIGO Scientific, Virgo), “Observation of Gravitational Waves from a Binary Black Hole Merger,” *Phys. Rev. Lett.* **116**, 061102 (2016), arXiv:1602.03837 [gr-qc].
- [10] Aldo Gamboa *et al.*, “Accurate waveforms for eccentric, aligned-spin binary black holes: The multipolar effective-one-body model SEOBNRv5EHM,” (2024), arXiv:2412.12823 [gr-qc].
- [11] Vijay Varma, Scott E. Field, Mark A. Scheel, Jonathan Blackman, Davide Gerosa, Leo C. Stein, Lawrence E. Kidder, and Harald P. Pfeiffer, “Surrogate models for precessing binary black hole simulations with unequal masses,” *Phys. Rev. Research* **1**, 033015 (2019), arXiv:1905.09300 [gr-qc].
- [12] Geraint Pratten, Cecilio García-Quiros, Marta Colleoni, Antoni Ramos-Buades, Héctor Estellés, Maite Mateu-Lucena, Rafel Jaume, Maria Haney, David Keitel, Jonathan E. Thompson, and Sascha Husa, “Computationally efficient models for the dominant and subdominant harmonic modes of precessing binary black holes,” *Physical Review D* **103** (2021), 10.1103/physrevd.103.104056.
- [13] C. M. Biwer, Collin D. Capano, Soumi De, Miriam Cabero, Duncan A. Brown, Alexander H. Nitz, and V. Raymond, “PyCBC Inference: A Python-based parameter estimation toolkit for compact binary coalescence signals,” *Publ. Astron. Soc. Pac.* **131**, 024503 (2019), arXiv:1807.10312 [astro-ph.IM].
- [14] Alex Nitz, Ian Harry, Duncan Brown, Christopher M. Biwer, Josh Willis, Tito Dal Canton, Collin Capano, Thomas Dent, Larne Pekowsky, Gareth S Cabourn Davies, Soumi De, Miriam Cabero, Shichao Wu, Andrew R. Williamson, Bernd Machenschalk, Duncan Macleod, Francesco Pannarale, Prayush Kumar, Steven Reyes, dfinstad, Sumit Kumar, Márton Tápai, Leo Singer, Praveen Kumar, veronica villa, maxtrevor, Bhooshan Uday Varsha Gadre, Sebastian Khan, Stephen Fairhurst, and Arthur Tolley, “gwastro/pycbc: v2.3.3 release of pycbc,” (2024).
- [15] Mark A. Scheel, Michael Boyle, Keefe Mitman, Nils Deppe, Leo C. Stein, Cristóbal Armaza, Marceline S. Bonilla, Luisa T. Buchman, Andrea Ceja, Himanshu Chaudhary, Yitian Chen, Maxence Corman, Károly Zoltán Csukás, C. Melize Ferrus, Scott E. Field, Matthew Giesler, Sarah Habib, François Hébert, Daniel A. Hemberger, Dante A. B. Iozzo, Tousif Islam, Ken Z. Jones, Aniket Khairnar, Lawrence E. Kidder, Taylor Knapp, Prayush Kumar, Guillermo Lara, Oliver Long, Geoffrey Lovelace, Sizheng Ma, Denyz Melchor, Marlo Morales, Jordan Moxon, Peter James Nee, Kyle C. Nelli, Eamonn O’Shea, Serguei Ossokine, Robert Owen, Harald P. Pfeiffer, Isabella G. Pretto, Teresita Ramirez-Aguilar, Antoni Ramos-Buades, Adhrit Ravichandran, Abhishek Ravishankar, Samuel Rodriguez, Hannes R. Rüter, Jennifer Sanchez, Md Arif Shaikh, Dongze Sun, Béla Szilágyi, Daniel Tellez, Saul A. Teukolsky, Sierra Thomas, William Throwe, Vijay Varma, Nils L. Vu, Marissa Walker, Nikolas A. Wittek, and Jooheon Yoo, “The sxs collaboration’s third catalog of binary black hole simulations,” (2025), arXiv:2505.13378 [gr-qc].
- [16] Keefe Mitman, Leo C Stein, Michael Boyle, Nils Deppe, Lawrence E Kidder, Harald P Pfeiffer, and Mark A Scheel, “Length dependence of waveform mismatch: a caveat on waveform accuracy,” *Classical and Quantum Gravity* **42**, 117001 (2025).
- [17] Gregory Ashton *et al.*, “BILBY: A user-friendly Bayesian inference library for gravitational-wave astronomy,” *Astrophys. J. Suppl.* **241**, 27 (2019), arXiv:1811.02042 [astro-ph.IM].
- [18] P. C. Peters, “Gravitational radiation and the motion of two point masses,” *Phys. Rev.* **136**, B1224–B1232 (1964).
- [19] Michael Zevin, Isobel M. Romero-Shaw, Kyle Kremer, Eric Thrane, and Paul D. Lasky, “Implications of eccentric observations on binary black hole formation channels,” *The Astrophysical Journal Letters* **921**, L43 (2021).
- [20] Isobel M. Romero-Shaw, Paul D. Lasky, Eric Thrane, and Juan Calderon Bustillo, “GW190521:

- orbital eccentricity and signatures of dynamical formation in a binary black hole merger signal,” *Astrophys. J. Lett.* **903**, L5 (2020), arXiv:2009.04771 [astro-ph.HE].
- [21] Marco Dall’Amico, Michela Mapelli, Stefano Torniamenti, and Manuel Arca Sedda, “Eccentric black hole mergers via three-body interactions in young, globular, and nuclear star clusters,” *Astron. Astrophys.* **683**, A186 (2024), arXiv:2303.07421 [astro-ph.HE].
- [22] Nihar Gupte *et al.*, “Evidence for eccentricity in the population of binary black holes observed by LIGO-Virgo-KAGRA,” (2024), arXiv:2404.14286 [gr-qc].
- [23] Khun Sang Phukon, Nathan K. Johnson-McDaniel, Amitesh Singh, and Anuradha Gupta, “Evolution of precessing binary black holes on eccentric orbits using orbit-averaged evolution equations,” (2025), arXiv:2504.20543 [gr-qc].
- [24] C. V. Vishveshwara, “Scattering of Gravitational Radiation by a Schwarzschild black-hole,” *Nature (London)* **227**, 936–938 (1970).
- [25] S. Chandrasekhar and Steven L. Detweiler, “The quasi-normal modes of the Schwarzschild black hole,” *Proc. Roy. Soc. Lond. A* **344**, 441–452 (1975).
- [26] Olaf Dreyer, Bernard J. Kelly, Badri Krishnan, Lee Samuel Finn, David Garrison, and Ramon Lopez-Aleman, “Black hole spectroscopy: Testing general relativity through gravitational wave observations,” *Class. Quant. Grav.* **21**, 787–804 (2004), arXiv:gr-qc/0309007.
- [27] Hengrui Zhu *et al.*, “Black hole spectroscopy for precessing binary black hole coalescences,” *Phys. Rev. D* **111**, 064052 (2025), arXiv:2312.08588 [gr-qc].
- [28] Maximiliano Isi, Matthew Giesler, Will M. Farr, Mark A. Scheel, and Saul A. Teukolsky, “Testing the no-hair theorem with GW150914,” *Phys. Rev. Lett.* **123**, 111102 (2019), arXiv:1905.00869 [gr-qc].
- [29] Eliot Finch and Christopher J. Moore, “Searching for a ringdown overtone in GW150914,” *Phys. Rev. D* **106**, 043005 (2022), arXiv:2205.07809 [gr-qc].
- [30] Yi-Fan Wang, Collin D. Capano, Jahed Abedi, Shilpa Kastha, Badri Krishnan, Alex B. Nielsen, Alexander H. Nitz, and Julian Westerweck, “A frequency-domain perspective on GW150914 ringdown overtone,” arXiv:2310.19645.
- [31] Collin D. Capano, Miriam Cabero, Julian Westerweck, Jahed Abedi, Shilpa Kastha, Alexander H. Nitz, Yi-Fan Wang, Alex B. Nielsen, and Badri Krishnan, “Multimode Quasinormal Spectrum from a Perturbed Black Hole,” *Phys. Rev. Lett.* **131**, 221402 (2023), arXiv:2105.05238 [gr-qc].
- [32] Harrison Siegel, Maximiliano Isi, and Will M. Farr, “Ringdown of GW190521: Hints of multiple quasinormal modes with a precessional interpretation,” *Phys. Rev. D* **108**, 064008 (2023), arXiv:2307.11975 [gr-qc].
- [33] Roberto Cotesta, Gregorio Carullo, Emanuele Berti, and Vitor Cardoso, “Analysis of Ringdown Overtones in GW150914,” *Phys. Rev. Lett.* **129**, 111102 (2022), arXiv:2201.00822 [gr-qc].
- [34] Swetha Bhagwat, Xisco Jimenez Forteza, Paolo Pani, and Valeria Ferrari, “Ringdown overtones, black hole spectroscopy, and no-hair theorem tests,” *Phys. Rev. D* **101**, 044033 (2020).
- [35] José Luis Jaramillo, Rodrigo Panosso Macedo, and Lamis Al Sheikh, “Pseudospectrum and black hole quasinormal mode instability,” *Phys. Rev. X* **11**, 031003 (2021).
- [36] Sizheng Ma, Keefe Mitman, Ling Sun, Nils Deppe, François Hébert, Lawrence E. Kidder, Jordan Moxon, William Throwe, Nils L. Vu, and Yanbei Chen, “Quasinormal-mode filters: A new approach to analyze the gravitational-wave ringdown of binary black-hole mergers,” *Phys. Rev. D* **106**, 084036 (2022).
- [37] Mark Ho-Yeuk Cheung *et al.*, “Nonlinear effects in black hole ringdown,” *Phys. Rev. Lett.* **130**, 081401 (2023).
- [38] Keefe Mitman *et al.*, “Nonlinearities in black hole ringdowns,” *Phys. Rev. Lett.* **130**, 081402 (2023).
- [39] Peter James Nee, Sebastian H. Völkel, and Harald P. Pfeiffer, “Role of black hole quasinormal mode overtones for ringdown analysis,” *Phys. Rev. D* **108**, 044032 (2023).
- [40] Vishal Baibhav, Mark Ho-Yeuk Cheung, Emanuele Berti, Vitor Cardoso, Gregorio Carullo, Roberto Cotesta, Walter Del Pozzo, and Francisco Duque, “Agnostic black hole spectroscopy: Quasinormal mode content of numerical relativity waveforms and limits of validity of linear perturbation theory,” *Phys. Rev. D* **108**, 104020 (2023).
- [41] Lionel London, Deirdre Shoemaker, and James Healy, “Modeling ringdown: Beyond the fundamental quasinormal modes,” *Phys. Rev. D* **90**, 124032 (2014), [Erratum: *Phys. Rev. D* **94**, 069902 (2016)].
- [42] Alex Correia and Collin D. Capano, “Sky marginalization in black hole spectroscopy and tests of the area theorem,” *Phys. Rev. D* **110**, 044018 (2024), arXiv:2312.15146 [gr-qc].
- [43] Alex Correia, Yi-Fan Wang, Julian Westerweck, and Collin D. Capano, “Low evidence for ringdown overtone in GW150914 when marginalizing over time and sky location uncertainty,” *Phys. Rev. D* **110**, L041501 (2024), arXiv:2312.14118 [gr-qc].
- [44] Robert E. Kass and Adrian E. Raftery, “Bayes Factors,” *J. Am. Statist. Assoc.* **90**, 773–795 (1995).
- [45] Francesco Nobili, Swetha Bhagwat, Costantino Pacilio, and Davide Gerosa, “Ringdown mode amplitudes of precessing binary black holes,” (2025), arXiv:2504.17021 [gr-qc].
- [46] James M. Bardeen, B. Carter, and S. W. Hawking, “The Four laws of black hole mechanics,” *Commun. Math. Phys.* **31**, 161–170 (1973).
- [47] S. W. Hawking, “Gravitational radiation from colliding black holes,” *Phys. Rev. Lett.* **26**, 1344–1346 (1971).
- [48] Shilpa Kastha, Collin D. Capano, Julian Westerweck, Miriam Cabero, Badri Krishnan,

- and Alex B. Nielsen, “Model systematics in time domain tests of binary black hole evolution,” *Phys. Rev. D* **105**, 064042 (2022), arXiv:2111.13664 [gr-qc].
- [49] Maximiliano Isi, Will M. Farr, Matthew Giesler, Mark A. Scheel, and Saul A. Teukolsky, “Testing the Black-Hole Area Law with GW150914,” *Phys. Rev. Lett.* **127**, 011103 (2021), arXiv:2012.04486 [gr-qc].
- [50] Miriam Cabero, Collin D. Capano, Ofek Fischer-Birnholtz, Badri Krishnan, Alex B. Nielsen, Alexander H. Nitz, and Christopher M. Biwer, “Observational tests of the black hole area increase law,” *Phys. Rev. D* **97**, 124069 (2018), arXiv:1711.09073 [gr-qc].
- [51] Collin D. Capano and Alexander H. Nitz, “Binary black hole spectroscopy: a no-hair test of GW190814 and GW190412,” *Phys. Rev. D* **102**, 124070 (2020), arXiv:2008.02248 [gr-qc].
- [52] Michael Zevin, Isobel M. Romero-Shaw, Kyle Kremer, Eric Thrane, and Paul D. Lasky, “Implications of Eccentric Observations on Binary Black Hole Formation Channels,” *Astrophys. J. Lett.* **921**, L43 (2021), arXiv:2106.09042 [astro-ph.HE].
- [53] Carl L. Rodriguez, Michael Zevin, Pau Amaro-Seoane, Sourav Chatterjee, Kyle Kremer, Frederic A. Rasio, and Claire S. Ye, “Black holes: The next generation—repeated mergers in dense star clusters and their gravitational-wave properties,” *Phys. Rev. D* **100**, 043027 (2019), arXiv:1906.10260 [astro-ph.HE].
- [54] Davide Gerosa and Emanuele Berti, “Escape speed of stellar clusters from multiple-generation black-hole mergers in the upper mass gap,” *Phys. Rev. D* **100**, 041301 (2019), arXiv:1906.05295 [astro-ph.HE].